Self-alignment of silicon chips on wafers: a capillary approach

J. Berthier[1], K. Brakke[2], F. Grossi[3], L. Sanchez[3], L. Di Cioccio[3]

[1] *CEA-LETI-Minatec, Department of Biotechnology, 17 avenue des Martyrs, 38954, Grenoble, France*

[2] *Mathematics Department, Susquehanna University, Selinsgrove, PA 17870-1164, USA*

[3] *CEA-LETI-Minatec, Department of Nanotechnology, 17 avenue des Martyrs, 38954, Grenoble, France*

As the limits of Moore's law are approached, 3D integration appears as the key to advanced microelectronic systems. Die-to-wafer assembly appears to be an unavoidable step to reach full integration. While robotic methods experience difficulties to accommodate fabrication speed and alignment accuracy, self-assembly methods are promising due to their parallel aspect which overcomes the main difficulties of current techniques. The aim of this work is the understanding of the mechanisms of self-alignment with an evaporating droplet technique. Stable and unstable modes are examined. Causes for misalignments of chips on wafers and their evolution are investigated with the help of the Surface Evolver numerical software. Precautions for suitable alignment are proposed.

I. INTRODUCTION

Integration of components on a wafer is needed to obtain fast and reliable packaging [1]. Self-assembly methods are promising due to their parallel aspect which overcomes the main difficulties of current techniques. It is expected that such methods could yield a higher assembly throughput rate and a higher alignment precision than conventional methods like robotic placement [2,3]. In this work we focus on the self-alignment of dies using droplets deposited on specific hydrophilic locations on the wafer. Capillary forces are used to align the die and evaporation of the liquid droplet eventually leads to contact and direct bonding of the die on the substrate [4-8]. This technique theoretically allows for self-alignment and assembly without any intermediate layer (Fig. 1). The bonding strength is high enough so that the assembly can handle post processing, such as thinning down or through-via etching for interconnects.

Experiments have been conducted with an experimental setup composed of dies on top of water droplets deposited with the help of a syringe on delimited regions of a substrate (Fig. 1). The die is a square plate of 5 mm x 5 mm, its thickness is 725 µm, and its weight is less than 45 mg. The silicon surface of the die is super-hydrophilic, with a water contact angle of the order of 2-3°. The substrate binding zone has the same size and is hydrophilically treated and surrounded by hydrophobic regions (Fig. 2). Note that the dimensional tolerance of die and pad conditions the alignment precision. Fabrication efforts are conducted to reach a dimensional tolerance less than 1 µm for the die as well as for the pad on the wafer. However in the numerical model, an ideal case is examined and the dimensional tolerance is set to zero.
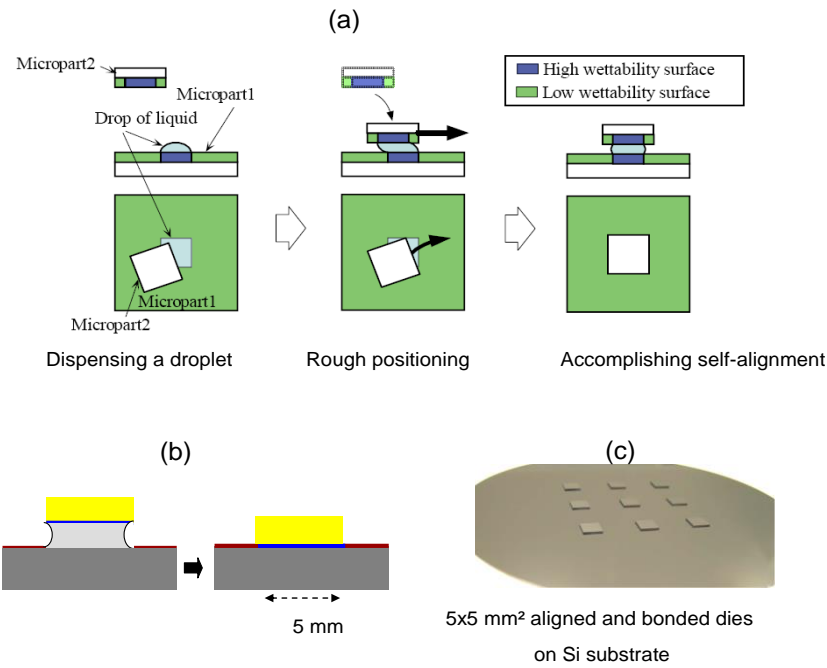
FIG. 1. Principle of die self-alignment: (a) sketch of the droplet and the die; (b) sketch of the die before and after evaporation; (c) view of aligned dies on a wafer [9].

The first experimental results have shown that good angular alignment is achieved, but a slight translational misalignment of the order of 10 to 20 µm can occur (Fig. 3). In previous publications [10,11], the possible reasons for misalignments have been experimentally investigated. We analyze here the self-alignment mechanism of the die on the wafer with the help of numerical simulation.

More specifically, our goal is to understand the details of the mechanisms of self-alignment and investigate the stable and unstable displacement modes. Using the characteristic times for capillarity, inertia and evaporation, we show that the self-alignment mechanism is governed by the capillary force exerted by the liquid-air surface.

FIG. 2. View of the boundary between the hydrophilic and hydrophobic regions; the bonding zone has been functionalized by oxygen plasma.
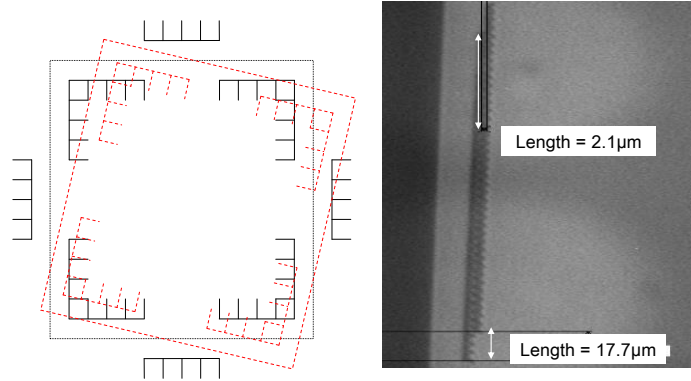

Length = 2.1μm

Length = 17.7μm

FIG. 3. Dicing marks (left) permit control of the alignment: a good angular alignment is reached, but a slight x-y shift may occur.

Hence the Surface Evolver software is well adapted for the analysis and prediction of the response of the system to misalignments and its evolution, e.g. whether the die re-aligns [12,13]. Let us recall that the Surface Evolver software uses a surface integral method which only requires meshing of the surface. It numerically determines the static—or quasi-static—location of an surface subject to mechanical constraints by an energy minimization approach. Note that fluid dynamics effects are not taken into account with this method. Typically in an Evolver calculation, a meshing of an arbitrary surface containing the liquid volume—here a

parallelepiped surface—is initially realized, and the surface evolves to reach an equilibrium state.

In a first step, the die is gently dropped on a water droplet sitting on a square hydrophilic pad patterned on the wafer surface. In a first approach, it is assumed that the release of the die does not induce an important inertial motion, i.e. the die is carefully placed on top of the droplet. At this point, three physical phenomena govern the die motion: (i) water-air surface forces that are expected to bring the die in an aligned position above its planned final location on the wafer, (ii) evaporation of the water that progressively moves the die towards the wafer surface, (iii) gravitational forces linked to the weight of the die and the liquid.

II. CHIP DISPLACEMENT MODES

Let us compare the characteristic times of the different mechanisms acting on the die: capillary, inertia and evaporation. The Tomotika time—or capillary time—is the time taken by a distorted liquid-air interface to regain its equilibrium shape against the action of the viscosity [14]. It is given by the ratio

$$\tau_{capillary} = \frac{\eta R}{\gamma},$$

where η is the fluid viscosity, R a characteristic dimension of the surface (here the vertical gap h), and γ the surface tension. Using a water viscosity value of $\eta = 10^{-3}$ Pa.s, a vertical gap $h = 20$ µm and a surface tension between water and air $\gamma = 72.10^{-3}$ N/m, we obtain $\tau_{capillary} < 10^{-6}$ seconds.

We can define an inertial time either based on the ratio between inertia and viscosity, or by

the ratio between inertia and capillarity. In the first case

$$\tau_{inertia} = \sqrt{\rho L^2 h / \eta V}$$

where h is the liquid thickness, L the dimension of the chip, ρ the density of the die and V the average velocity of the die during its motion. V is obtained from experiment and is of the order of $V \sim 0.1$ mm/s, and typically $h=20$ µm, $L=5$ mm. In the second case

$$\tau_{inertia} = \sqrt{\rho L^2 h / \gamma} .$$

The two inertia times are respectively of the order of 7 and 0.01 seconds.

Finally we derive an evaporation time based on the diffusion of vapor [15]. The mass transfer equation is

$$\frac{dm}{dt} = D \frac{\partial c}{\partial n} 4 h L$$

where D is the diffusion coefficient, c the vapor concentration, n the normal unit vector and m the mass of liquid: $m = \rho_w h L^2$, ρ_w being the density of the liquid. An approximation of the vapor gradient of concentration is $\frac{\partial c}{\partial n} \approx \frac{c_{sat}}{L}$, where c_{sat} is the saturation concentration (concentration at the interface). It can be shown that

$$\tau_{evap} \approx \frac{L^2}{4 D} \frac{\rho_w}{c_{sat}} .$$

Physical tables indicate the approximate values: $D = 21.10^{-6}$ m/s^2 and $c_{sat} = 1.2$ kg/m^3. The evaporation time is then $\tau_{evap} \approx 250$ seconds. This value is in agreement with experiments showing complete evaporation after 4 to 5 minutes. Hence $\tau_{capillary} \ll \tau_{inertia} \ll \tau_{evap}$. The displacement of the die is then governed by capillary forces linked to the minimization of the liquid surface area along with the forces exerted by the liquid and die weight under the constraint of constant volume [16,17]. The surface energy of the droplet is given by

$$E_T = \gamma_{WA} S_{WA} + \gamma_{SW} S_{SW} + \gamma_{DW} S_{DW} \qquad (1)$$

where S_{WA}, S_{SW}, S_{DW} are respectively the surface areas of the water-air interface, substrate-water interface and die-water interface, and $\gamma_{WA}, \gamma_{SW}, \gamma_{DW}$ are the surface tensions between water and air, substrate and water, and die and water. We make the simplifying hypothesis that the droplet is pinned on the die edges on its top, and on the contour line of the hydrophilic pad on its bottom. Hence, the contact angles do not intervene and the energy to be minimized is that of gravitational potential plus the water-air interface energy $E = \gamma_{WA} S_{WA}(x, y, z, \theta, \alpha, \phi, P, \gamma)$, where x,y,z are the coordinates of the mass center of the die, θ, α, ϕ the direction angles of the die, P the weight of the die and γ the surface tension between water and air. We use the Surface Evolver to follow the displacement of the die towards its stable position minimizing the total energy.

Four different displacement modes can be identified (Fig. 4): (1) shift, which is a horizontal translation of the plate, (2) twist, corresponding to a rotation of the plate in the horizontal plane, (3) lift, corresponding to a vertical motion of the plate, and (4) tilt and roll, which are respectively rotations around the horizontal y-axis and x-axis.
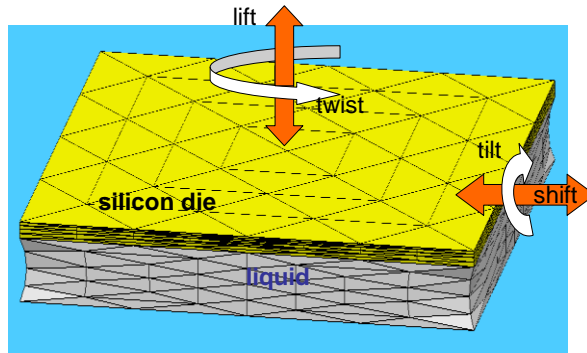
FIG. 4. The four different modes (and possible reasons for misalignment): lift, twist, shift and tilt.

We investigate successively these four modes and check if each of these modes is subject to self-alignment.

Our approach is twofold: numerical with Surface Evolver and analytical approximation of the shapes by simplified surfaces. In the first case, the weight of the die is taken into account (but it is so small that it has hardly any consequences); in the second case the weight of the die is not taken into account. In the analytical models, we implicitly use the property that the ratio between liquid thickness and die dimensions is small: $h/L \ll 1$.

A. First mode: horizontal displacement (shift)

Let us denote by S the surface area, and by V_l the liquid volume. The first displacement mode corresponds to a horizontal shift of the die (Fig. 5). It is obvious that the surface area is larger after a shift. Consequently the capillary forces will act to reduce the surface area by bringing the die back into alignment.

A calculation with the Surface Evolver shows that strong capillary forces pull back the die into alignment. The force along the horizontal direction x is given by

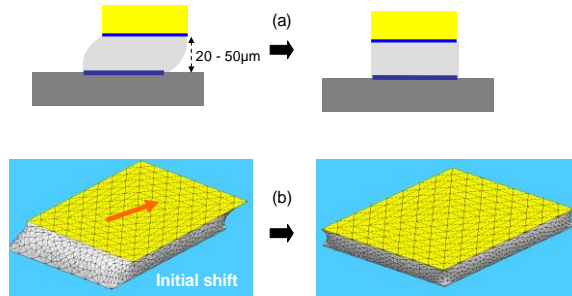$$F_x = -\frac{\partial(\gamma S)}{\partial x}.$$

(2)

FIG. 5. (a) After a horizontal displacement, the die is restored to alignment by capillary forces; (b) Evolver calculation of the pullback.

Fig. 6 shows the values of the restoring force for different liquid gaps. In the case of small shifts, this force is larger for small gaps because of the larger relative change of surface area.
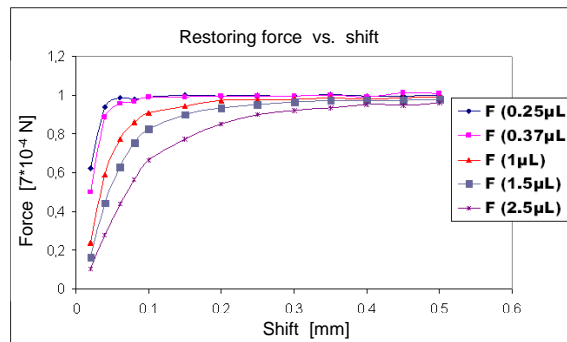
FIG. 6. Restoring force vs. shift for different values of the droplet volume.

This behavior can be checked against an approximate model where the surfaces would be planar (which is not exactly true). Under this assumption, it can be easily shown (Appendix A) that the liquid-air surface energy is approximately

$$E \approx 2\gamma h L \left(1 + \sqrt{1 + \left(\frac{x}{h}\right)^2}\right), \tag{3}$$

where x is the horizontal shift, and the capillary force is

$$F_x \approx -2\gamma L \frac{1}{\sqrt{1 + \left(\frac{h}{x}\right)^2}}. \tag{4}$$

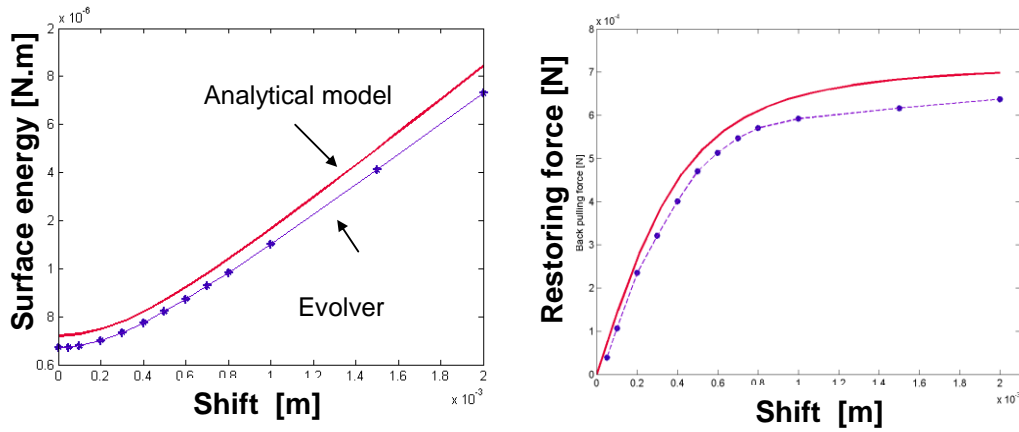This formula compares well with Evolver results, as shown in Fig. 7.

FIG. 7. Comparison between approximate analytical model (plain line) and Evolver (dots).

Left: surface energy; right: restoring force.

The energy curves in Fig. 7 show that the real surface area at zero shift—calculated with Evolver—is a little smaller than that corresponding to four planar surfaces ($S = 4 h L$). This is linked to the shape of the surface, corresponding to a minimal surface area. For very small shifts, $x/h \ll 1$ and $F_x \approx -2\gamma L x/h$: the restoring force is a linear function of the shift; for large shifts $x/h \gg 1$, $F_x \approx -2\gamma L$ and the restoring force is constant. An important observation

stemming from Eq. (4) and from Evolver results is that the restoring force is larger for small vertical gaps h.

B. Second mode: rotation around z-axis (twist)

A twist is a rotation around the vertical z-axis. In this case too, a twist increases the surface area, and the die is pulled back to alignment, as shown in Fig. 8. As for the shift, we have approached the problem by using the Surface Evolver and comparing the results to an approximate analytical model where the surfaces—initially planar—are twisted progressively (Appendix B).
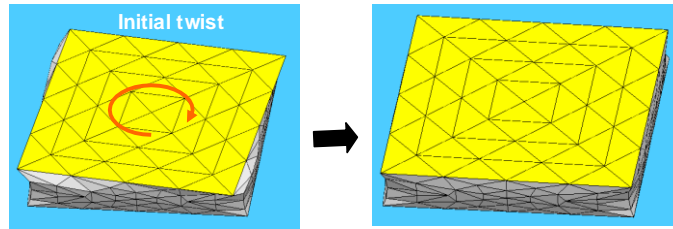
FIG. 8. Die realigns after an initial twist.

Let us recall that the torque on the die is given by

$$T = -\frac{\partial(\gamma S)}{\partial \theta}.$$
(5)

Surface energy and torque are plotted in Fig. 9 as functions of the twist angle for three different liquid heights (100, 200 and 500 µm).
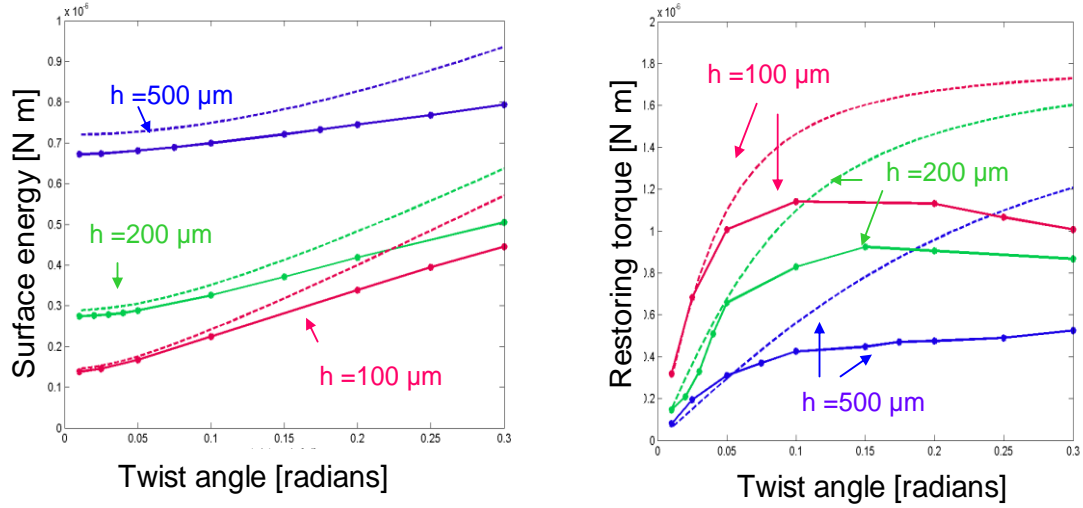
FIG. 9. Energy (left) and torque (right) as functions of the twist angle, for three values of the gap. Dotted lines are Surface Evolver results and plain lines correspond to the analytical model.

The surface energy is obviously larger for larger gaps; also the derivative with respect to the twist angle is larger for smaller gaps, i.e. the variation of surface area with the twist angle is larger in the case of smaller gaps. Hence, the torque is larger for smaller liquid volumes. The analytical model produces a torque value given by

$$T \approx \gamma L^2 \left[\frac{a}{\sqrt{1+a^2}} + \frac{1}{\left(a+\sqrt{1+a^2}\right)}\left(\frac{1}{a}+\frac{1}{\sqrt{1+a^2}}\right) - \frac{\ln\left(a+\sqrt{1+a^2}\right)}{a^2} \right] , \qquad (6)$$

with $a = L\theta/(2h)$. For small twists, the analytical model compares well with the Evolver, but not for large twists. In this latter case, the surface is considerably affected by surface tension forces and the hypothesis used by the analytical model is not physical. In such a case an Evolver numerical approach is essential to predict the real shape of the surfaces and consequently deduce the values of the torque.

C. Third mode: vertical displacement (lift)

Because the vertical location of the die is a balance between gravity and capillary forces, it is expected that there is only one stable height for the die. This height depends on the liquid volume and die weight. This analysis recalls the work of Suzuki [18]. This is confirmed by Evolver numerical simulation (fig.10). The surface energy is shown in Fig. 11 and the restoring force in Fig. 12. In each figure, a comparison has been made between Evolver results and a simplified approach based on a circular curvature of the surfaces (see Appendix C).
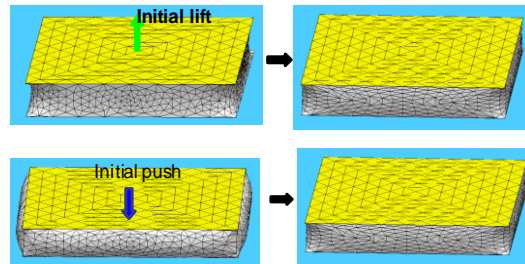
FIG. 10. The die regains its stable position after a lift. Top: after an initial lift; bottom: after an initial compression.
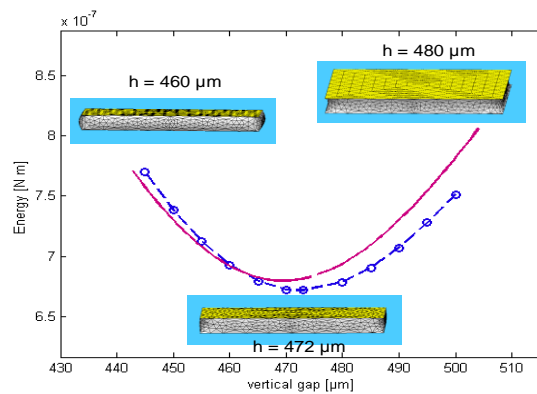

FIG. 11. Surface energy as a function of the vertical gap: The continuous line corresponds to the analytical model and the dotted line to Evolver results.
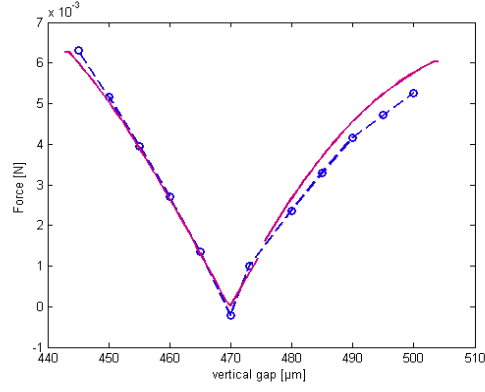
FIG. 12. Restoring force vs. vertical gap. Continuous line: analytical model; dotted line: Evolver results.

D. Fourth mode: tilt (or roll)

D.1. Physical analysis

We will call tilt a rotation around the y-axis and roll a rotation around the x-axis. Basically, tilt and roll share the same behavior. Besides, in our case where the chip has a square shape, tilt and roll are exactly identical. Tilt is a complex phenomenon because the variation of the surface area is more difficult to intuitively predict. If we make the very simple calculation depicted in Fig. 13, we deduce that the problem is indeterminate. For the same volume of the same liquid, assuming the simplest form of surfaces, the surface energy in a flat configuration is

$$E = \gamma\, S = \gamma\left(4\, L\, h\right) = \gamma\left(4\frac{V_l}{L}\right), \tag{7}$$

where V_l is the liquid volume. In a dihedral morphology, the surface energy is

$$E = \gamma S = \gamma \left[2\left(\frac{\alpha L^2}{2} \right) + \alpha L^2 \right] = \gamma \left(4\frac{V_l}{L} \right) . \qquad (8)$$

Hence, it is the distortion of the surfaces that can make the difference and pinpoint the stable position. It is a second order problem. This remark leads to serious complications: from a numerical standpoint, the meshing of the surface should be sufficiently fine to produce a precise value of the energy. In return, the computation time is long. From a physical standpoint, the role of the parameters—like the weight of the die, or the surface tension of the liquid—is difficult to predict.
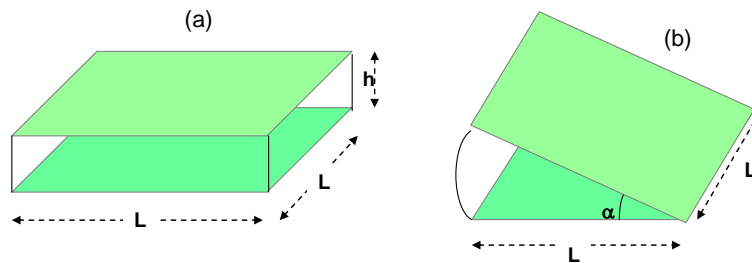

FIG. 13. Two morphologies of the liquid having the same surface energy.

The numerical model shows that the dihedral position (b in figure 14) is the stable position whatever the initial depth of the liquid gap.
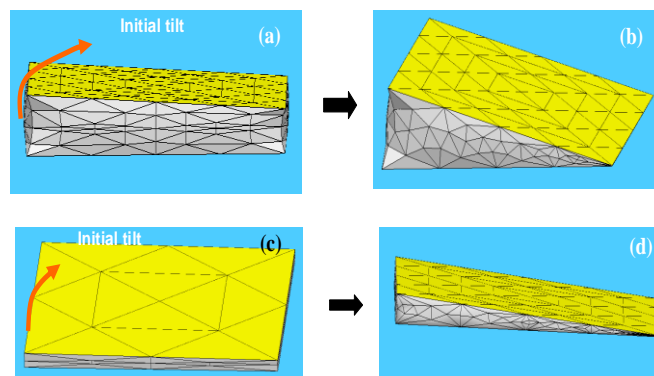

FIG. 14. Die tilts to form a dihedral: (a) and (b) large liquid volume; (c) and (d) small liquid volume.

Surface energy and torque obtained numerically with the Surface Evolver are plotted in figures 15 and 16. The horizontal lines correspond to the analytical approximation.
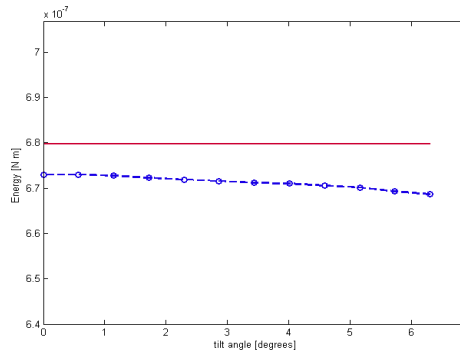

FIG. 15. Comparison between Evolver numerical program and analytical model: in case of tilt, the interfacial energy varies extremely slowly.
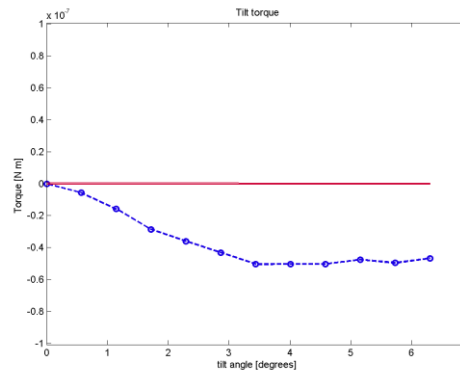

FIG. 16.Tilt torque vs. tilt angle: continuous line indicates a zero torque, and the Evolver results (dotted line) show a small tilting torque.

The slightly smaller surface area for the dihedral morphology is due to small distortions of the surface in the die corners and along the die sides. The surface is concave in the corners, and convex along the sides (Fig. 17). Parallel die-wafer morphology has 4 concave and 4 convex distortions, whereas the dihedral die-wafer morphology has only 2 concave and 3 convex distortions.
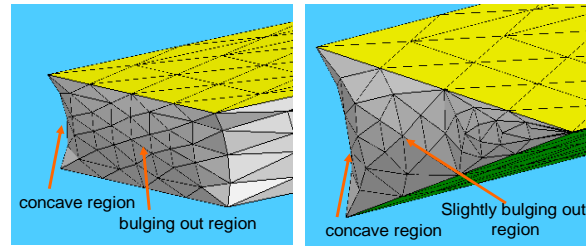
FIG. 17. Bulging out/in shape of the surface in the two cases: left, parallel plates; right, dihedral.

D.2. Chip Sliding

In the case we are considering in this paper, the ratio h/L is very small, of the order of 10^{-3}. In this paragraph, for completeness, we extend our investigation to large volumes of liquid-i.e. the liquid thickness is of the order or larger than the chip dimensions ($h/L > 0.5$). Note that such a large liquid thickness usually results in overflowing, which will be studied in section III. Tilt associated to large liquid thickness, triggers the sliding of the chip as shown in figure 18. In such a case, a translational misalignment occurs after evaporation. It is also observed that sliding is enhanced by the chip weight.
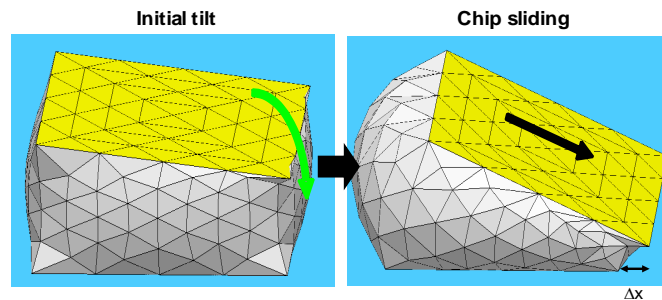

FIG. 18. The chip may slide after a tilt in the case of a large volume of liquid and/or a heavy chip weight.

D.3. Wetting of the pad corners

Let us continue our investigations on the tilt mode. Even for very hydrophilic surfaces, corners are never totally wetted (fig. 19). It is shown in Appendix D that the horizontal curvature radius of the triple line in a corner is of the order of half the liquid thickness (h/2). Hence, it is expected that four dewetted regions exist in the four corners of the pad. This point is experimentally confirmed. In the case of tilt, the numerical model shows that the dewetted regions become progressively smaller on the sides where the chip comes closer to the pad and, conversely, larger where the chip gets farther from the pad (fig.19). This property is enhanced by the weight of the pad. Such a configuration favors the formation of a small translational misalignment depending on the not-wetted surface areas.
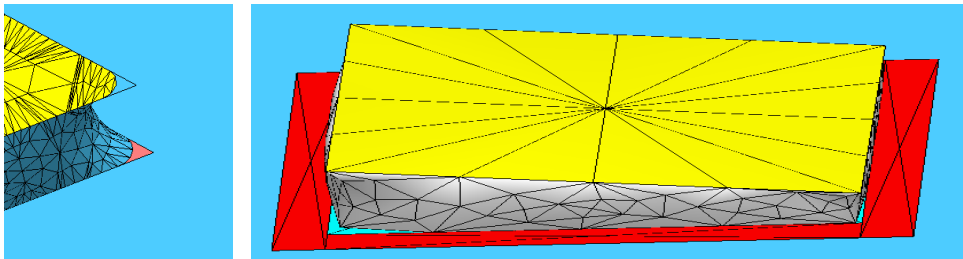

FIG.19. Left: corners are never totally wetted. Right: picture of the chip after a tilt with the dewetted corners.

D.4. Discussion on the tilt mode

In conclusion, it has been shown that the tilt mode is slightly unstable, resulting in the slow formation of a dihedral. When the liquid thickness is very small compared to the dimension of the chip, an aligned dihedral is formed.

Misalignment may occur in the case of large liquid volume and large chip weight. Misalignments are also promoted by large dewetted zones in the pad corners. Super-hydrophilicity of the pad and small chip weight reduce the potential of tilt misalignment.

E. Coupled modes

From the previous analysis, it is expected that only coupled modes including roll and tilt will be unstable. This can be verified with the Surface Evolver (Fig. 20). This software calculates an equilibrium state and does not compute a dynamic motion. However, the iteration speed indicates a relative facility or difficulty of displacement. For a tilt and roll initial displacement (Fig. 20.a), there is first a slow motion of the plate that accelerates until one corner and then an edge of the chip contacts the substrate. After that, the motion is slow to form a complete dihedral. In the case of an initial tilt and twist (Fig. 20.b), the twist vanishes quickly (it is a stable mode) but the tilt slowly increases. Finally, for an initial shift and twist—which are two stable modes—the shift vanishes first, then the twist (Fig. 20.c).
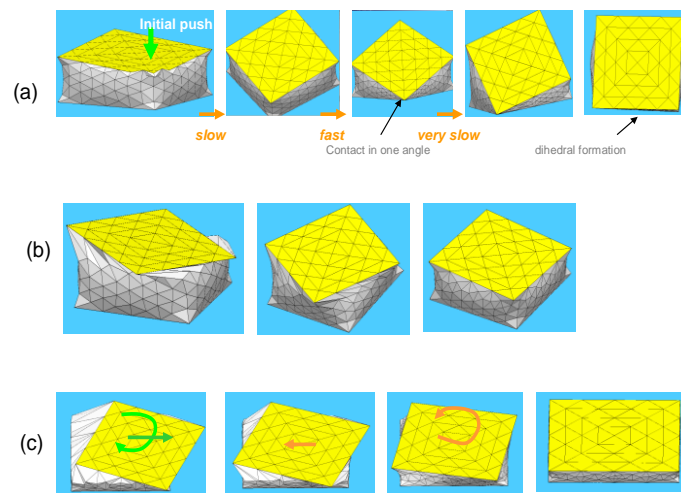

FIG. 20. Coupled modes: (a): tilt and roll; (b) tilt and twist; (c) shift and twist. The only unstable coupling must include a tilt and/or roll; the other modes are automatically corrected by the capillary forces.

III. DROPLET CONFINEMENT

The results obtained in the preceding section are rather favorable for chip self-alignment, as only one mode—the tilt—is very slightly unstable, all the others producing a large restoring force or torque. If we take into account that the liquid height is very small compared to the horizontal dimensions of the chip (h/L <1/100), we have to look elsewhere for the observed causes of misalignment. It is clear that droplet confinement on the hydrophilic pad is of utmost importance. It has been experimentally observed that any spreading of the contact line outside the hydrophilic pad boundaries results in a systematic misalignment (Fig. 21). In order to avoid spreading, a strong wetting contrast must exist between the hydrophilic pad and the wafer. Indeed, the surface must not surpass the canthotaxis limit [17]. This limit can behave differently if the wafer surface is planar or has relief. In the first case, the canthotaxis limit is given by the maximum possible bulging of the surface—which is the Young angle of the hydrophobic wafer—whereas in the second case, it is given by the Young angle on the vertical side of the pillar plus the pillar angle—usually 90° (Fig. 22). Note that in the latter case, the pillar edge must be sharp or else the canthotaxis limit decreases [19].

The largest possible bulging angle of the liquid is difficult to determine. It depends on the weight of the die, and also on the way the die is placed on top of the droplet. In this case, inertia—which has been so far neglected—could have an important effect. Hence, the limit depends on the protocol and should be determine experimentally.
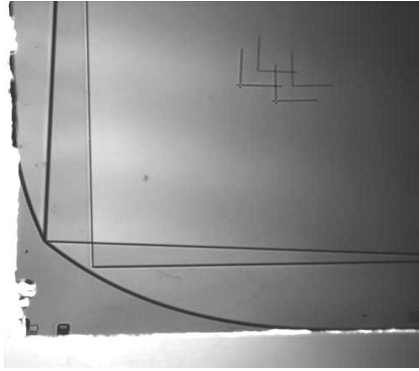
FIG. 21. Misalignment due to water spreading on the wafer outside the hydrophilic pad. The die makes a 10° twist, plus a shift with the pad.
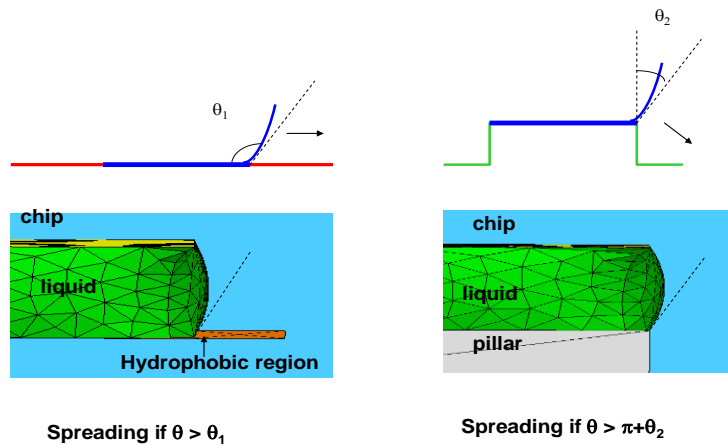

Spreading if $\theta > \theta_1$

Spreading if $\theta > \pi + \theta_2$

FIG. 22. (Color online) Canthotaxis limits for planar wafer and wafer with relief.

IV. CONCLUSIONS

Of all the four modes, only the tilt (roll) is weakly unstable. However, this latter mode should not constitute a drawback for self-alignment. First, because the liquid layer thickness and the chip weight are small, it is expected that the dihedral will form correctly without misalignment, as shown in Fig. 14. Second, the tilt-motion mode is extremely slow when the

die weight is small; evaporation might proceed simultaneously, reducing further the liquid volume. This point is still under investigation.

This work has shown that de-pinning is probably the most important cause of misalignment: if the liquid overflows over the hydrophobic surface, the alignment has no reason to be good. In order to avoid liquid spreading, a sharp wetting contrast must be established between the pad and the rest of the wafer. Two different approaches can be made to reinforce the wetting contrast: first, a hydrophobic treatment of the wafer; second, the use of relief. In both cases, it requires an initial treatment of the wafer that must take into account the direct bonding that takes place when the water has evaporated. One has to be especially cautious at the moment when the die is placed on top of the droplet. An inertial motion of the die could be transmitted to the liquid and might trigger spreading. This point is presently under investigation.

ACKNOWLEDGEMENTS

APPENDIX A: SHIFT ENERGY AND RESTORING FORCE

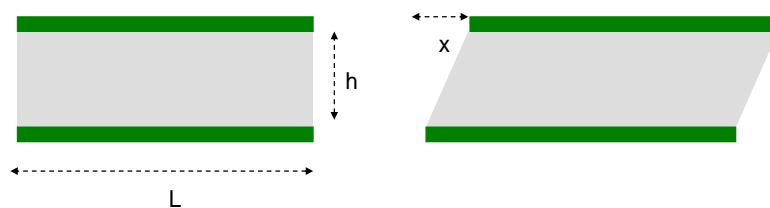In this appendix, planar surfaces are assumed. The shift is then sketched in Fig. 23.

FIG. 23. (Color online) Sketch of the shift: left, at alignment; right, after a shift.

The volume of the liquid is then

$$V_l = h L^2 .$$ (A.1)

And the surface area at alignment is given by

$$S_1 = \frac{4V_l}{L} .$$ (A.2)

With the same assumption of planar surfaces, the surface area with a shift x is

$$S_2 = \frac{2V_l}{L}\left(1+\sqrt{1+\left(\frac{x}{h}\right)^2}\right) = 2hL\left(1+\sqrt{1+\left(\frac{x}{h}\right)^2}\right).$$ (A.3)

Note that when $x \rightarrow 0$, $E \rightarrow 4\gamma h L.$ The surface energy difference $\Delta E = \gamma\left(E_2 - E_1\right)$ is

$$\Delta E = \gamma\left(\frac{2V_l}{L}\right)\left(\sqrt{1+\left(\frac{x}{h}\right)^2} - 1\right).$$ (A.4)

The restoring force is then

$$F_x \approx -2\gamma L \frac{1}{\sqrt{1+\left(\frac{h}{x}\right)^2}} .$$ (A.5)

APPENDIX B: TWIST ENERGY AND RESTORING TORQUE

In this appendix, the four surfaces are supposed to be planar at alignment, having square angles between each other. Recall that a twist around the z axis by angle θ corresponds to the rotation matrix

$$R = \begin{pmatrix} \cos\theta & -\sin\theta \\ \sin\theta & \cos\theta \end{pmatrix}. \tag{B.1}$$

The twist can be sketched as in Figs. 24 and 25. In order to obtain a twist of angle θ, we suppose that the horizontal sections are progressively twisted from $z=0$ to $z=h$, by an angle of $\frac{z}{h}\theta$.

For a fixed y, the base point M $(s,y,0)$ describes a spiral curve defined by

$$\tilde{M} = \begin{pmatrix} s\,\cos\left(\frac{z}{h}\theta\right) - y\sin\left(\frac{z}{h}\theta\right) \\ s\,\sin\left(\frac{z}{h}\theta\right) + y\cos\left(\frac{z}{h}\theta\right) \\ z \end{pmatrix}. \tag{B.2}$$
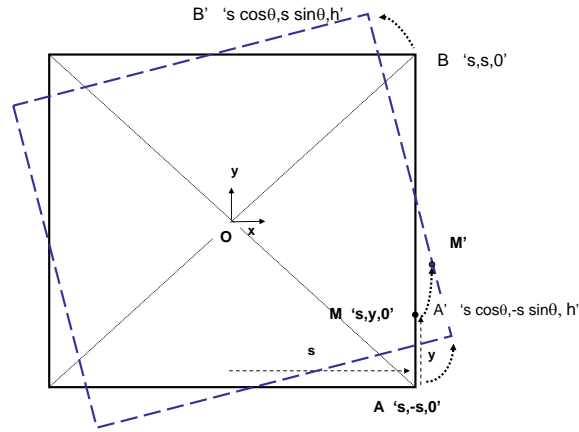
FIG. 24. Sketch of the twist. The point M is describing AB while M' is describing A'B'. Note that $s=L/2$.
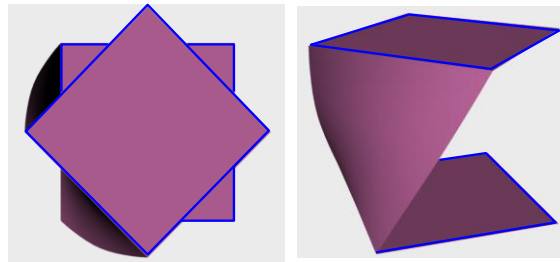

FIG. 25. (Color online) Three dimensional view of the twisted surface (only one twisted surface is shown in the figure).

Let us consider the parametric vector function $\vec{f}$ such as

$$
\vec{f}:[-s,s]\times[0,h]\to\Re^{3}, \qquad (y,z)\to
\begin{pmatrix}
s\ \cos\left(\dfrac{z}{h}\theta\right)-y\sin\left(\dfrac{z}{h}\theta\right)\\[2mm]
s\ \sin\left(\dfrac{z}{h}\theta\right)+y\cos\left(\dfrac{z}{h}\theta\right)\\[2mm]
z
\end{pmatrix}. \qquad\text{(B.3)}
$$

This function produces the coordinates of $\tilde{M}$. The infinitesimal surface ds is given by

$$ds = \left\| \frac{\partial \vec{f}}{\partial y} \times \frac{\partial \vec{f}}{\partial z} \right\| dy \, dz \; . \tag{B.4}$$

Using the calculated values

$$\frac{\partial \vec{f}}{\partial y} = \begin{pmatrix} -\sin\left(\frac{z}{h}\theta\right) \\ \cos\left(\frac{z}{h}\theta\right) \\ 0 \end{pmatrix} ,$$

$$\frac{\partial \vec{f}}{\partial z} = \begin{pmatrix} -\frac{\theta}{h}\left[s \, \sin\left(\frac{z}{h}\theta\right) + y \cos\left(\frac{z}{h}\theta\right)\right] \\ \frac{\theta}{h}\left[s \, \cos\left(\frac{z}{h}\theta\right) - y \sin\left(\frac{z}{h}\theta\right)\right] \\ 1 \end{pmatrix} . \tag{B.5}$$

The vector product $\dfrac{\partial \vec{f}}{\partial y} \times \dfrac{\partial \vec{f}}{\partial z}$ is then

$$\frac{\partial \vec{f}}{\partial y} \times \frac{\partial \vec{f}}{\partial z} = \begin{pmatrix} \cos\left(\frac{z}{h}\theta\right) \\ \sin\left(\frac{z}{h}\theta\right) \\ \frac{\theta}{h}\left[-\sin\left(\frac{z}{h}\theta\right)\left(s \cos\left(\frac{z}{h}\theta\right) - y \sin\left(\frac{z}{h}\theta\right)\right) \right. \\ \left. + \cos\left(\frac{z}{h}\theta\right)\left(s \sin\left(\frac{z}{h}\theta\right) + y \cos\left(\frac{z}{h}\theta\right)\right)\right] \end{pmatrix} \tag{B.6}$$

which can be simplified to

$$\frac{\partial \vec{f}}{\partial y} \times \frac{\partial \vec{f}}{\partial z} = \begin{pmatrix} \cos\left(\frac{z}{h}\theta\right) \\ \sin\left(\frac{z}{h}\theta\right) \\ \frac{\theta}{h}y \end{pmatrix}. \tag{B.7}$$

The infinitesimal surface ds is finally

$$ds = \left\| \frac{\partial \vec{f}}{\partial y} \times \frac{\partial \vec{f}}{\partial z} \right\| dy\, dz = \sqrt{1 + \left(\frac{y}{h}\theta\right)^2}\, dy\, dz. \tag{B.8}$$

And the surface area (for one surface) is

$$A = \int_{z=0}^{z=h} \int_{y=-s}^{y=s} \sqrt{1 + \left(\frac{y}{h}\theta\right)^2}\, dy\, dz = h \int_{y=-s}^{y=s} \sqrt{1 + \left(\frac{y}{h}\theta\right)^2}\, dy = \theta \int_{y=-s}^{y=s} \sqrt{\left(\frac{h}{\theta}\right)^2 + y^2}\, dy. \tag{B.9}$$

Using the table for irrotational functions integrals [20], we find a total surface energy of

$$E = 4\gamma \left[s\,h\sqrt{1+a^2} + \frac{h^2}{\theta}\ln\left(a + \sqrt{1+a^2}\right) \right],$$
$$a = \frac{s\,\theta}{h}. \tag{B.10}$$

Note that when $\theta \to 0$, $a \to 0$ and $E \to E = 4\gamma\,L\,h$. The torque T is given by the derivative of

the energy with respect to the angle θ

$$T = 4\gamma s^2 \left[\frac{a}{\sqrt{1+a^2}} + \frac{1}{\left(a+\sqrt{1+a^2}\right)}\left(\frac{1}{a} + \frac{1}{\sqrt{1+a^2}}\right) - \frac{\ln\left(a+\sqrt{1+a^2}\right)}{a^2} \right]. \tag{B.11}$$

APPENDIX C: LIFT ENERGY AND RESTORING FORCE

It is assumed that the chip is lifted up or down from its equilibrium position $y \neq h_0$. Let us calculate the surface area using the simplifying hypothesis that each of the four surfaces has a circular profile as shown in Fig. 26. The total surface area is then

$$S = 4L(2\theta R), \tag{C.1}$$

and the (constant) droplet volume is

$$V = L^2 h_0 = L^2 y - 4L\left(\theta R^2 - \frac{y}{2}R\cos\theta\right). \tag{C.2}$$

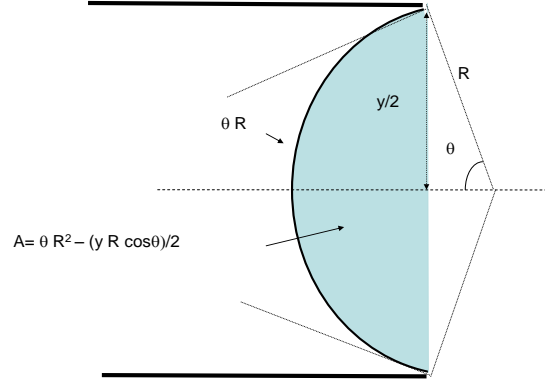Using the relation

$$R = \frac{y}{2\sin\theta}, \tag{C.3}$$

FIG. 26. Sketch of the surface.

we find

$$L^2 h_0 = L^2 y - L\frac{y^2}{\sin\theta}\left(\frac{\theta}{\sin\theta} - \cos\theta\right) \qquad \frac{\pi}{2} > \theta > 0$$

$$L^2 h_0 = L^2 y + L\frac{y^2}{\sin\theta}\left(\frac{\theta}{\sin\theta} - \cos\theta\right) \qquad \pi > \theta > \frac{\pi}{2}.$$

(C.4)

For a given angle θ, this last relation is a quadratic polynomial in y which root is

$$y = \frac{L - L\sqrt{1 - 4\frac{2}{\sin\theta}\left(\frac{\theta}{\sin\theta} - \cos\theta\right)L h_0}}{\frac{2}{\sin\theta}\left(\frac{\theta}{\sin\theta} - \cos\theta\right)} \qquad if \; \frac{\pi}{2} > \theta > 0.$$

$$y = \frac{-L + L\sqrt{1 + 4\frac{2}{\sin\theta}\left(\frac{\theta}{\sin\theta} - \cos\theta\right)L h_0}}{\frac{2}{\sin\theta}\left(\frac{\theta}{\sin\theta} - \cos\theta\right)} \qquad if \; \pi > \theta > \frac{\pi}{2}.$$

(C.5)

APPENDIX D: CURVATURE RADIUS OF THE TRIPLE LINE IN A CORNER

Laplace's theorem in the middle of the chip edge yields the relation

$$\Delta P = \gamma \left(\frac{1}{R_1} + \frac{1}{R_2} \right) \approx \gamma \left(\frac{1}{R_2} \right) \tag{D.1}$$

where R_1 and R_2 are respectively the horizontal and vertical curvature radii of the surface. Laplace's theorem for the surface curvature in a corner is

$$\Delta P = \gamma \left(\frac{1}{R_h} - \frac{1}{R_v} \right) = \gamma \left(\frac{1}{R_2} \right) \tag{D.2}$$

where R_h and R_v are respectively the horizontal and vertical curvature radii of the surface in the corner. From (D.1) and (D.2), we derive

$$\frac{1}{R_h} = \frac{1}{R_v} + \frac{1}{R_2} \tag{D.3}$$

Because the weight of the die is small, it is observed that $R_v \ll R_2$ (fig.19, left) the horizontal curvature radius in the corner is approximately

$$R_h \approx R_v \tag{D.4}$$

The vertical radius of curvature R_v being of the order of $h/2$, then

$$R_h \approx \frac{h}{2} \tag{D.5}$$

Hence an order of magnitude of the curvature radius of the triple line in a corner is half the liquid thickness.

References

[1] M. Koyanagi, T. Fukushima, T. Tanaka. Proc. of the 2009 Conference on Asia and South Pacific Design and Automation, Yokohama, Japan, 19-22 December 2009, pp. 409-415.

[2] http://www.datacon.at/

[3] http://www.set-sas.fr/en/

[4] T. Fukushima, T. Tanaka, M. Koyanagi. Proc. Advanced Metallization Conference, pp 479-485, 2009.

[5] H.J. Yeh, J.S. Smith. IEEE Photonics Technology Letters, **6** (6), 706 (1994)

[6] W. Zheng, H.O. Jacobs. Advanced Functional Materials, **15** (5), 2005, 732 (2005).

[7] H. Moriceau, B. Bataillou, C. Morales, A.M. Cartier, F. Rieutord. 7th Intl. Symp. on Semiconductor Wafer Bonding. ECS Proceedings, **19**, 49 (2003).

[8] Q.Y. Tong, U. Gösele. *Semiconductor Wafer Bonding* (John Wiley and Sons 1999).

[9]. K. Sato, T. Seki, S. Hata, A. Shimokohbe. Precision Engineering, **27**, 42 (2003).

[10]. F. Grossi, L. Di Cioccio, F. Rieutord, O. Renault, J. Berthier, J-C Barbé, F. De Crécy and L. Clavelier. Proc. MRS Fall Meeting, Boston, USA, 1-5 December 2008.

[11]. F. Grossi, L. Di Cioccio, S. Vincent, M.D. Diop, L. Bally, N. Kernevez, F. Rieutord. Proc. Imaps Conference, Scottsdale, USA, March 19-22, 2007

[12] K. Brakke. Exp. Math., **1**, 141 (1992).

[13] http://www.susqu.edu/brakke/evolver/evolver.html

[14] J. Berthier, P. Silberzan. *Microfluidics for Biotechnology*, 2nd ed. (Artech House , 2010).

[15] K.S. Birdi, D.T. Vu, A. Winter, "A study of the evaporation rate of small water drops placed on a solid surface," J. Phys. Chem., Vol. 93, pp. 3702 -3703, 1989

[16]. A. Greiner, J. Lienemann, J.G. Korvink, X. Xiong, Y. Hanein, K.F. Bohringer. Proc. Int. Conf. on modeling and Simulation of Microsystems, 2002.

[17]. J. Berthier. *Microdrops and Digital Microfluidics*. (William Andrew Publishing, February 2008).

[18]. K. Suzuki. Microsystem Technology, **11**, 1107 (2005).

[19] J. Berthier, F. Loe-Mie, V.-M. Tran, S. Schoumacker, F. Mittler, G. Marchand, N. Sarrut. J. Coll. Int. Sci., **338**, pp. 296–303, 2009.

[20] M. Abramowitz and I.A. Stegun. Handbook of Mathematical Functions with Formulas, Graphs, and Mathematical Tables.

 http://www.math.ucla.edu/~cbm/aands//intro.htm#006